Thermodynamics and Mechanism of α Helix Initiation in Alanine and Valine Peptides†

Douglas J. Tobias‡ and Charles L. Brooks III*
Department of Chemistry, Carnegie Mellon University, Pittsburgh, Pennsylvania 15213
Received December 7, 1990; Revised Manuscript Received March 22, 1991

ABSTRACT: We used molecular dynamics simulations to study the folding/unfolding of one turn of an α helix in Ac-$(Ala)_3$-NHMe and Ac-$(Val)_3$-NHMe. Using specialized sampling techniques, we computed free energy surfaces as functions of a conformational coordinate that corresponds to α helices at small values and to extended conformations at large values. Analysis of the peptide conformations populated during the simulations showed that α helices, reverse turns, and extended conformations correspond to minima on the free energy surfaces of both peptides. The free energy difference between α helix and extended conformations, determined from the equilibrium constants for helix unfolding, is approximately −1 kcal/mol for Ac-$(Ala)_3$-NHMe and −5 kcal/mol for Ac-$(Val)_3$-NHMe. The mechanism observed in our simulations, which includes reverse turns as important intermediates along the helix folding/unfolding pathway, is consistent with a mechanism proposed previously. Our results predict that both peptides (but especially the Ala peptide) have a much larger equilibrium constant for helix initiation than is predicted by the helix–coil transition theory with the host–guest parameters. We also predict a much greater difference in the equilibrium constants than the theory predicts. Insofar as helix initiation is concerned, our results suggest that the large difference between the helical propensities of Ala and Val cannot be explained by simple concepts such as side-chain rotamer restriction or unfavorable steric interactions. Rather, the origin of the difference appears to be quite complicated because it involves subtle differences in the solvation of the two peptides. The two peptides have similar turn–extended equilibria but very different helix–turn equilibria, and the difference in helical propensities reflects the fact that the helix–turn equilibrium strongly favors the turns in Ac-$(Val)_3$-NHMe, while it favors the helices in Ac-$(Ala)_3$-NHMe. We also computed thermodynamic decompositions of the free energy surfaces, and these revealed that the helix–turn equilibria are vastly different primarily because the changes in peptide–water interactions that accompany helix-to-turn conformational changes are qualitatively different for the two peptides.

Right-handed helices are the most prevalent secondary structural element in proteins of known structure. In their survey of the X-ray atomic coordinates of 57 proteins, Barlow and Thornton (1988) found that 35% of the residues were involved in helices [by the definition of Kabsch and Sander (1983)]. Of the helices identified by Barlow and Thornton (1988), 80% were α helices, which generally have around 3.6 residues per turn, with the backbone atoms in each turn forming a 13-atom ring closed by a hydrogen bond between the CO group of residue i and the NH group of residue i+4. The remainder (20%) were 3_{10} helices, which have three residues per turn, with each turn forming a 10-atom ring closed by a tilted hydrogen bond between residues i and i+3. In globular proteins, the side chains of residues in helices often alternate from hydrophobic to hydrophilic with a periodicity of three to four, giving the helices an amphipathic character (Schiffer & Edmundson, 1967; Richardson, 1981).

Helices in globular proteins are stabilized by a variety of interactions. Commonly located along the outside of proteins, helices are stabilized by interactions of polar groups on their outer face with solvent and by the packing of apolar groups on their inner face in the protein interior. Helices can also be stabilized by i to i+4 amide hydrogen bonds, by salt bridges, and/or by interactions of their partially charged ends with oppositely charged side chains ["charge–helix dipole interactions" (Shoemaker et al., 1985)]. However, when separated from the remainder of the protein, small peptides corresponding to stable helices in proteins usually do not form stable isolated helices in solution. Evidently, the primary reason for this is the loss of stabilizing packing interactions. There is only a handful of short peptides known to form stable isolated helices in solution when separated from proteins: S-peptide, C-peptide, and synthetic analogues from ribonuclease A (Klee, 1968; Bierzynski et al., 1982) and Pα5, the α helix from BPTI (Goodman & Kim, 1989). In all of these cases, helical conformations are stabilized in solution by sequence-specific interactions such as salt bridges (Bierzynski et al., 1982; Kim et al., 1982; Marqusee & Baldwin, 1987; Goodman & Kim, 1989; Osterhout et al., 1989) or charge–helix dipole interactions (Shoemaker et al., 1985, 1987; Fairman et al., 1989; Goodman & Kim, 1989; Bradley et al., 1990).

Because there are only a few peptides that are known to form stable helices when removed from proteins, the question of whether or not individual amino acids have intrinsic propensities toward the formation of small helices in solution has been difficult to answer. In an attempt to answer this question, many researchers have studied helix formation in various series of so-called de novo designed peptides (Marqusee & Baldwin, 1987, Marqusee et al., 1989; Padmanabhan et al., 1990; Bradley et al. 1990; O'Neil & DeGrado, 1990; Lyu et al., 1990). O'Neil and DeGrado (1990) and Lyu et al. (1990) obtained very similar scales for the effects of amino acid

† This work was partially supported by an NIH grant to C.L.B. (GM37554). C.L.B. was an A. P. Sloan Foundation Fellow (1990–1992). D.J.T. was supported by an NIH predoctoral training grant.
* To whom correspondence should be addressed.
‡ Present address: Department of Chemistry, University of Pennsylvania, Philadelphia, Pennsylvania 19104.

0006-2960/91/0430-6059$02.50/0

substitution on the relative free energies of helix formation, and they concluded that the concept of intrinsic helical propensities is valid. In contrast, Padmanabhan et al. (1990) concluded that "the helix-forming tendency of a particular amino acid depends on the sequence context in which it occurs." Thus, questions concerning the validity of the concept of intrinsic helical propensities, and the physical forces determining them if they exist, have yet to be thoroughly answered.

Another question that has not been adequately answered is, What are the mechanism and time scale for the folding and unfolding of helices in solution? This question is difficult to address experimentally because the techniques [nuclear magnetic resonance (NMR) and circular dichroism (CD) spectroscopy] used to detect helical conformations find equilibrium populations of folded and unfolded structures. Thus, the helices are fully formed on the time scales of the experiments. The answers to the above questions are crucial for assessing and refining current theories of protein folding.

Many currently popular models for the folding process are based on the "framework model" (Ptitsyn & Rashin, 1975; Richmond & Richards, 1978; Kim & Baldwin, 1982), according to which the initial stages of folding involve the formation of marginally stable secondary structures, such as reverse turns or small stretches of helices. Once formed, these structures can direct the folding process by greatly reducing the conformational space available to the folding polypeptide chain and by bringing together residues that are distant in sequence (Zimmerman & Scheraga, 1977). The initiation structures can either coalesce and grow or be rearranged into different structures, as tertiary interactions take place. The framework model is supported by the direct observation of "framework" intermediates (Udgaonkar & Baldwin, 1988; Roder et al., 1988) as well as the observation that stable secondary structures form in small peptides of native sequence under folding conditions (Dyson et al., 1988). Further detailed studies of secondary structure formation will certainly enhance our understanding of the initial events of protein folding and, hence, folding mechanisms. In this paper, we consider the topic of α helix formation in small peptides in solution.

To date, several researchers have made observations which suggest that helix folding/unfolding occurs through reverse-turn intermediates. On the basis of their observation that the terminal residues in helices also frequently occur in reverse turns, Blagdon and Goodman (1975) proposed that helix formation might be initiated at the termini by turns. Recently, Sundaralingam and Sekharudu (1989) suggested a similar mechanism for helix folding/unfolding based on their analysis of helix hydration in protein crystal structures. Since water-inserted helical segments display a variety of reverse-turn conformations, Sundaralingam and Sekharudu (1989) claimed that the turns could be considered as trapped intermediates along the helix folding/unfolding pathway. Subsequently, DiCapua et al. (1990) reported that water insertion into the O_3–N_7 hydrogen bond of a deca-alanine helix in solution led to both "transient" (~15 ps) and "persistent" (~70 ps) destabilization of the helix during a 100-ps molecular dynamics (MD) simulation at 300 K. Very recently, Tirado-Rives and Jorgensen (1990) carried out MD simulations of a small peptide in water that provided additional information regarding helix stability and the process of helix unfolding in solution. They found, in agreement with Bierzynski et al. (1982), that a fifteen residue S-peptide analogue formed stable helices in water at low temperature (278 K), but the helices unfolded at a much higher temperature (358 K). Moreover, Tirado-Rives and Jorgensen observed that the helix unfolding took place in a few hundred picoseconds at 358 K, and the breakup and re-formation of helical hydrogen bonds occurred on a time scale of several hundred picoseconds through 3_{10} helix or reverse-turn intermediates.

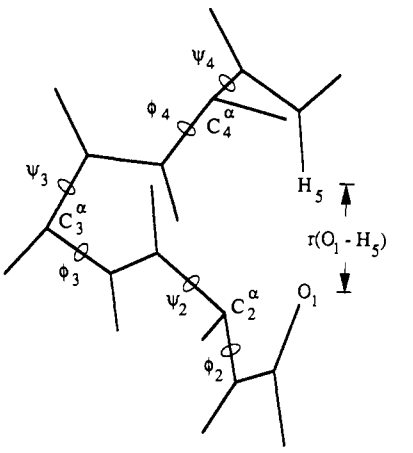

FIGURE 1: Pseudoatom model of the Ac-$(Ala)_3$-NHMe peptide used in this study, in a right-handed α helical conformation, with the folding/unfolding reaction coordinate $r(O_1$–$H_5)$ and the backbone dihedral angles (ϕ_i,ψ_i) indicated.

In order to learn more about the stability and folding mechanisms of α helices, we have carried out molecular dynamics simulations of the folding/unfolding of one turn of an α helix in Ac-$(Ala)_3$-NHMe (Ac is the amino-terminal blocking group $COCH_3$, and NHMe is the carboxy-terminal blocking group $NHCH_3$) in water. We studied the folding/unfolding by defining the one-dimensional *reaction coordinate* $r(O_1$–$H_5)$ as the distance between the Ac (first "residue") carbonyl oxygen and the NHMe (fifth "residue") amide hydrogen and carrying out a series of simulations of the peptide with that distance constrained at different values (Figure 1). At small values of $r(O_1$–$H_5)$, the peptide forms a well-defined single turn of an α helix, and at large values the peptide is fully extended. Using the "umbrella sampling" formalism (Valleau & Torrie, 1977; Tobias et al., 1991a), we have computed the free energy as a function of $r(O_1$–$H_5)$ from the biased probability distributions generated in our constrained simulations. We have used our results to quantitatively assess the relative stability of helical, extended, and stable intermediate structures along the unfolding reaction coordinate, to estimate the rates of interconversion of these structures, and to propose a mechanism for one-turn helix folding/unfolding. In addition, we have used a thermodynamic decomposition of the free energies to interpret the relative stabilities of the stable structures in terms of differences in peptide–peptide and peptide–water interactions. Of course, since we have only studied one turn of a helix, our results are strictly applicable only to the processes of helix initiation or the breakup of an isolated helical hydrogen bond. Nonetheless, our results are consistent with the predictions of Sundaralingam and Sekharudu (1989) and the observations of Tirado-Rives and Jorgensen (1990) regarding the mechanism for the formation and breakup of α helical hydrogen bonds during helix folding/unfolding.

Marqusee et al. (1989) observed that 16-residue alanine-based peptides, solubilized by the insertion of three or more residues of a single-charge type (Lys or Glu), formed very stable helices in water at 274 K. They showed that the helices were not stabilized by association or by charge–helix dipole interactions, and they concluded that individual alanine residues have a high helical propensity of unknown origin. The

observation that short alanine-based helices (or more generally, any short helices) are stable in solution is in marked contrast to the predictions made by using the Zimm–Bragg theory of the helix–coil transition (Zimm & Bragg, 1959) with parameters determined from "host–guest" experiments (Wojcik et al., 1990). The results of the present study also demonstrate, insofar as helix initiation is concerned, that helix formation in alanine peptides is much more favorable than is predicted by using the Zimm–Bragg theory. Padmanabhan et al. (1990) recently studied helix formation in a series of 17-residue alanine-based peptides with 1–3 Ala residues substituted by Ile, Leu, Phe, or Val. They found that substitution of Ala by a β branched or aromatic residue substantially lowered the helix-forming tendency of the peptide. Furthermore, the results of Padmanabhan et al. (1990) differed from the predictions of the theory both in the order and the magnitude of variation of the helix-forming tendencies of the peptides. The origins of the relative stabilities of the helices were not obvious in the study of Padmanabhan et al. In an attempt to determine the origin of the exceptional helical propensity of Ala (e.g., compared to Val), we have also used contrained MD simulations to study helix folding/unfolding in Ac-$(Val)_3$-NHMe. We computed the free energy surface and its thermodynamic decomposition along the $r(O_1–H_5)$ coordinate for the Val peptide and compared them to the corresponding results for the Ala peptide.

Materials and Methods

The simulation methods used here are similar to those used by Tobias et al. (1991a) to study reverse-turn unfolding. We studied the folding/unfolding of one-turn α helices in Ac-$(Ala)_3$-NHMe and Ac-$(Val)_3$-NHMe by carring out series of simulations with the $O_1–H_5$ distance, $r(O_1–H_5)$, constrained near particular values. We initially built each peptide in one turn of an idealized right-handed [$\phi_i \approx -60°$, $\psi_i \approx -60°$ (Richardson, 1981)] α helix, with $r(O_1–H_5) \approx 1.9$ Å. Then we minimized the energy of the peptides in vacuum using the CHARMM potential energy function and parameters [all of the energy minimizations and molecular dynamics simulations described herein were carried out using the CHARMM program (Brooks et al., 1983)] with a dielectric constant $\epsilon = 40$ and with the addition of a harmonic constraint potential, $U^*(r)$,

$$U^*(r) = K(r - r_0)^2 \quad (1)$$

where the force constant $K = k_BT/[2(\delta r)^2]$, e.g., δr is the deviation, from the reference distance r_0, at which the constraint energy is $k_BT/2$ (in the present work, we used δr = 0.2–0.3 Å). The constraint potential is supposed to keep the separation $r(O_1–H_5)$ near r_0 during the course of minimization (or dynamics). At the end of the energy minimizations, the peptides were still in well-defined helical conformations, with $r(O_1–H_5) \approx 1.9$ Å. From each minimized peptide, we generated another structure with a larger value of $r(O_1–H_5)$ by increasing the value of r_0 and repeating the minimization. We repeated this procedure for the Ala peptide, generating each new structure from the most recently generated one, until we had a set of 18 structures with $r(O_1–H_5)$ in the range 1.8–11.0 Å. When we looked at the structures generated using this procedure, we found that small values of $r(O_1–H_5)$ correspond to a turn of an α helix and intermediate values to reverse turns. The structures with large values of $r(O_1–H_5)$ were partially extended, with the three sets of flexible backbone dihedral angles (ϕ_i,ψ_i) in the α, α, and β regions of the Ramachandran map (Richardson, 1981). Since our intention was to study the equilibrium between helical (all α) and fully extended (all β) structures, we used an alternative procedure to generate the large $r(O_1–H_5)$ starting structures. We began with all β extended structure [$\phi_i \approx -90°$, $\psi_i \approx 140°$, $r(O_1–H_5) \approx 10.2$ Å] and generated eight structures with $r(O_1–H_5)$ in the range 8.0–11.4 Å using a series of constrained minimizations. The structure with $r(O_1–H_5) \approx 8.0$ Å was very similar to the twelfth structure [$r(O_1–H_5) \approx 7.4$ Å] from the first series. Thus, we used 12 structures from the first series and the 8 structures from the second series as starting structures for the continuous transformation of Ac-$(Ala)_3$-NHMe from helix to fully extended conformations. We used the same procedure to generate 20 structures of the Val peptide with $r(O_1–H_5)$ in the range 1.8–11.4 Å. Finally, to prepare for the solution simulations, each structure was placed in the center of a rectangular box of water molecules, and the solvent molecules that overlapped with the peptide were removed.

In principle, conformational equilibria in peptides could be studied by using a single computer simulation if all configurations corresponding to the full range of values of the important degrees of freedom could be adequately sampled. In practice, this is generally impossible since the system tends to get trapped in wells on the potential energy surface, and transitions between wells across high-energy barriers (more than a few times the thermal energy) are usually rare during the course of a feasible simulation. One way to circumvent this problem is to use a specialized sampling technique known as umbrella sampling. In the umbrella sampling procedure (Valleau & Torrie, 1977; Tobias et al., 1991a), an auxiliary "umbrella" potential $U^*(r)$ is added to the potential energy function of the system to bias the sampling toward a desired range of the reaction coordinate r. When a series of simulations in which $U^*(r)$ is systematically varied is carried out, statistics are gathered in a series of overlapping "windows" centered around different values of r. The resulting biased probability distributions are subsequently corrected to remove the effects of $U^*(r)$ and used to compute pieces of the free energy surface $W_i(r)$ in each window. Finally, the $W_i(r)$ from overlapping windows are matched to form a continuous free energy surface or "potential of mean force" (pmf), which we denote as $W(r)$. However, the resulting pmf contains an additive constant, and, therefore, the absolute vertical location of the overall pmf computed by this procedure is unknown. Since we will restrict ourselves to a discussion of the shapes of the surfaces and free energy differences taken from the surfaces, the absolute vertical locations are not important. Finally, we note that the formalism used to calculate the pmfs contains no approximations. Errors in the pmfs arise from finite sampling of the probability distributions and statistical uncertainties in the averages.

The relative stability of two particular conformations may be determined by calculating the difference between two points on a pmf. However, when the relative stability of two *states* is desired, the free energy difference between ensembles of conformations must be computed. If one wants to know the relative stability of two states, X and Y, which correspond to two distributions of conformations (e.g., helical and extended structures), then one should compute the free energy difference ΔA^{XY} from the equilibrium constant for the conversion of X to Y, K_{eq}^{XY}:

$$\Delta A^{XY} = A(Y) - A(X) = -k_BT \ln K_{eq}^{XY} \quad (2)$$

The equilibrium constant is simply the ratio of the mole fractions of X and Y, X_X and X_Y, which can be computed by integrating populations determined from the pmf (Zichi & Rossky, 1986; Tobias et al., 1991a). One should be careful about interpreting equilibrium constants, and relative free energies computed from them, because the results are often

quite sensitive to the choice of the ranges of integration, which is somewhat arbitrary.

In order to understand the relative free energies of different conformations in solution in terms of microscopic interactions, it is useful to decompose free energy differences into energetic and entropic contributions arising from differences in peptide–peptide and peptide–water interactions (Tobias et al., 1991a). The Helmholtz free energy difference between two conformational states X and Y may be written

$$\Delta A^{XY} = \Delta E - T\Delta S \quad (3)$$

where ΔE and ΔS are the differences in internal energy and entropy, respectively. The internal energy difference is equal to the difference of the average potential energies, which may be written as the sum of average peptide–peptide, peptide–water, and water–water interaction energy differences (Tobias et al., 1991a). Similarly, the entropy difference may be decomposed into a configurational contribution arising from the peptide conformational fluctuations within the free energy wells (Karplus et al., 1987) and peptide–water and water–water contributions that are comprised of complicated averages over peptide–water and water–water interactions, respectively (Yu & Karplus, 1988). The water–water energetic and entropic contributions exactly cancel for each conformation, and therefore they do not contribute to the free energy difference (Yu & Karplus, 1988). Thus, the thermodynamic decomposition may be written

$$\Delta A^{XY} = \langle \Delta U_{uu} \rangle + \langle \Delta U_{uv} \rangle - T\Delta S_{c,uv} \quad (4)$$

where $\langle \Delta U_{uu} \rangle$ and $\langle \Delta U_{uv} \rangle$ are the average peptide–peptide and peptide–water interaction energy differences, respectively, and $\Delta S_{c,uv}$ is the sum of the peptide configurational and peptide–water entropy differences. For the potential energy function we use, the peptide–peptide interaction energy differences contain contributions from bond, angle, torsion, van der Waals, and electrostatic energies, while the peptide–water differences contain only van der Waals and electrostatic contributions. It is straightforward to compute the average interaction energies but difficult to calculate the entropy difference directly from the simulation data. Since the entropy contribution is the only missing term in eq 4, we obtain it indirectly as the difference between ΔA and the average interaction energies. Since we will consider differences between two ensembles of conformations that have particular values of the reaction coordinate and the fluctuations of the unconstrained degrees of freedom are similar in the two ensembles, we assume that the difference in configurational entropy is small (Karplus et al., 1987). Therefore, we will assume that $\Delta S_{c,uv}$ is composed primarily of the difference in peptide–water entropy.

We carried out molecular dynamics simulations on each of the solvated peptide systems constructed and constrained as described above. Each system consisted of one peptide molecule and 194–196 water molecules in a cubic box with periodic boundary conditions. We used the three-site TIP3P model of Jorgensen et al. (1983) for water. The box side length was 18.856 Å, yielding approximate agreement with the experimentally observed room temperature water density (1.0 g·cm^{-3}) after the solute volume was subtracted from the box volume. The nonbonded energies and forces were smoothly truncated at 7.75 Å [using a van der Waals switching function and an electrostatic shifting function (Brooks et al., 1983)], based on atomic centers, according to the minimum image convention (Allen & Tildesley, 1989). The Verlet (1967) algorithm was used to integrate Newton's equations of motion (with a time step of 1.5 fs). Each of the simulations consisted of 10 000 steps (15 ps) of equilibration and 20 000 steps (30 ps) of data collection. The nonbonded interactions were processed by using a list-based algorithm (Verlet, 1967), and the lists were updated every 10 steps. The velocities were periodically reassigned from a Maxwell–Boltzmann distribution to maintain temperatures of approximately 300 K. The SHAKE constraint algorithm (Ryckaert et al., 1977) was used to keep the water molecules rigid and to maintain rigid N–H bonds in the peptide molecules. All of the remaining degrees of freedom were allowed to fluctuate. The coordinates of each system were stored every five time steps for the calculation of the pmfs, equilibrium constants, and other statistical properties that are presented and discussed below. The simulations were carried out on the Cray YMP computer at the Pittsburgh Supercomputing Center.

Results

In this section we present our results for the free energy surfaces and their thermodynamic decompositions. In addition to computing the free energy surfaces, we have further analyzed our trajectories to see what peptide conformations were generated by the constrained molecular dynamics simulations. We present the results of this analysis first, so that we can identify regions of the reaction coordinate with particular peptide conformations in the remainder of this paper. We used the joint probability densities of the pairs of dihedral angles (ϕ_2,ψ_2), (ϕ_3,ψ_3), and (ϕ_4,ψ_4) to characterize the peptide backbone conformations and distributions of O–N distances to characterize the hydrogen bonding during several constrained simulations along the helix folding/unfolding pathway. We will show that certain regions of the reaction coordinate $r(O_1–H_5)$ correspond to helical, reverse-turn, and extended peptide conformations. In Figures 2 and 3 we present the normalized probability densities of the dihedral angles from three simulations of each peptide.

The dihedral angle distributions (Figures 2 and 3) show that both the Ala and Val peptides maintained α helical conformations (Figure 1) throughout the r_0 = 2.2 Å simulations: the distributions are all peaked in the α region of the Ramachandran-type map (Richardson, 1981). The most probable values of (ϕ_2,ψ_2), (ϕ_3,ψ_3), and (ϕ_4,ψ_4) are (−80°,−40°), (−80°,−40°), and (−80°,−60°) for Ac-$(Ala)_3$-NHMe (Figure 2) and (−80°,−60°), (−80°,−40°), and (−80°,−60°) for Ac-$(Val)_3$-NHMe (Figure 3). In addition, the probability distributions of the $O_1–N_5$ distance (not shown) are sharp and centered at ~3 Å, indicating the presence of α helical hydrogen bonds for both peptides. The biased probability distributions of the $O_1–H_5$ distance (not shown) from the r_0 = 2.2 Å simulations covered the range 1.8–2.2 Å and were centered at 2.0 Å. Thus, we identify α helical conformations with the region $r(O_1–H_5) \approx 2$ Å.

In Figures 2 and 3 we can see that the (ϕ_2,ψ_2) and (ϕ_3,ψ_3) pairs of dihedral angles in both peptides occupied the α region throughout the r_0 = 4.0 Å simulations. The (ϕ_4,ψ_4) pair was exclusively β for the Val peptide and mostly β for the Ala peptide. However, for the the Ala peptide, the (ϕ_4,ψ_4) pair also spent a considerable amount of time in the α region and in the "neck" region between α and β. Using molecular graphics, we observed that, although the backbone dihedral angles were predominantly in the α helical region, most of the structures from the r_0 = 4.0 Å simulations were nonideal type I [by the criterion of Richardson (1981)] or type III [by the criterion of Chou and Fasman (1977)] reverse turns involving residues 1–4 (Figure 4A,C). Furthermore, we observed that the Ala peptide also occasionally populated similar turn conformations involving residues 2–5 (Figure 4B). To characterize

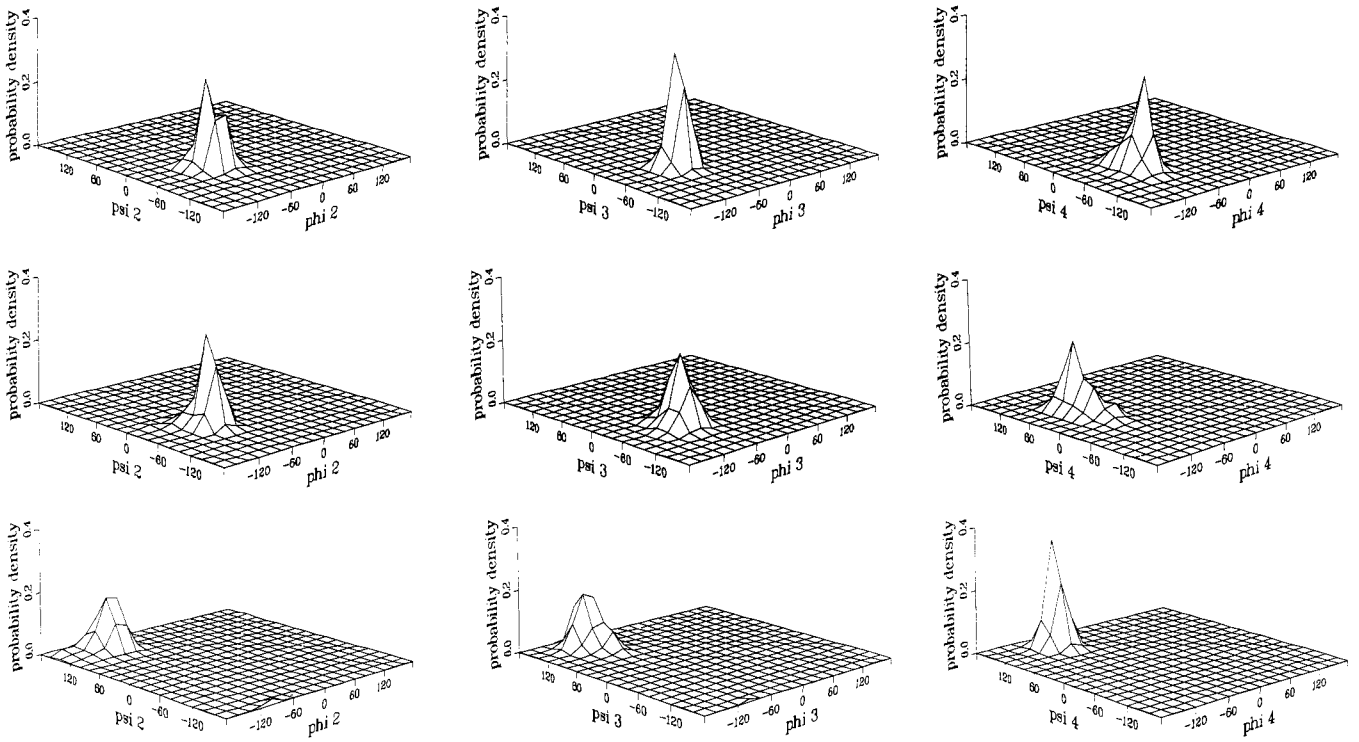

FIGURE 2: Normalized joint probability densities of the dihedral angle pairs (ϕ_2,ψ_2), (ϕ_3,ψ_3), and (ϕ_4,ψ_4) for Ac-(Ala)$_3$-NHMe. The top set of distributions is from the r_0 = 2.2 Å simulation, the middle from the r_0 = 4.0 Å simulation, and the bottom from the r_0 = 10.2 Å simulation.

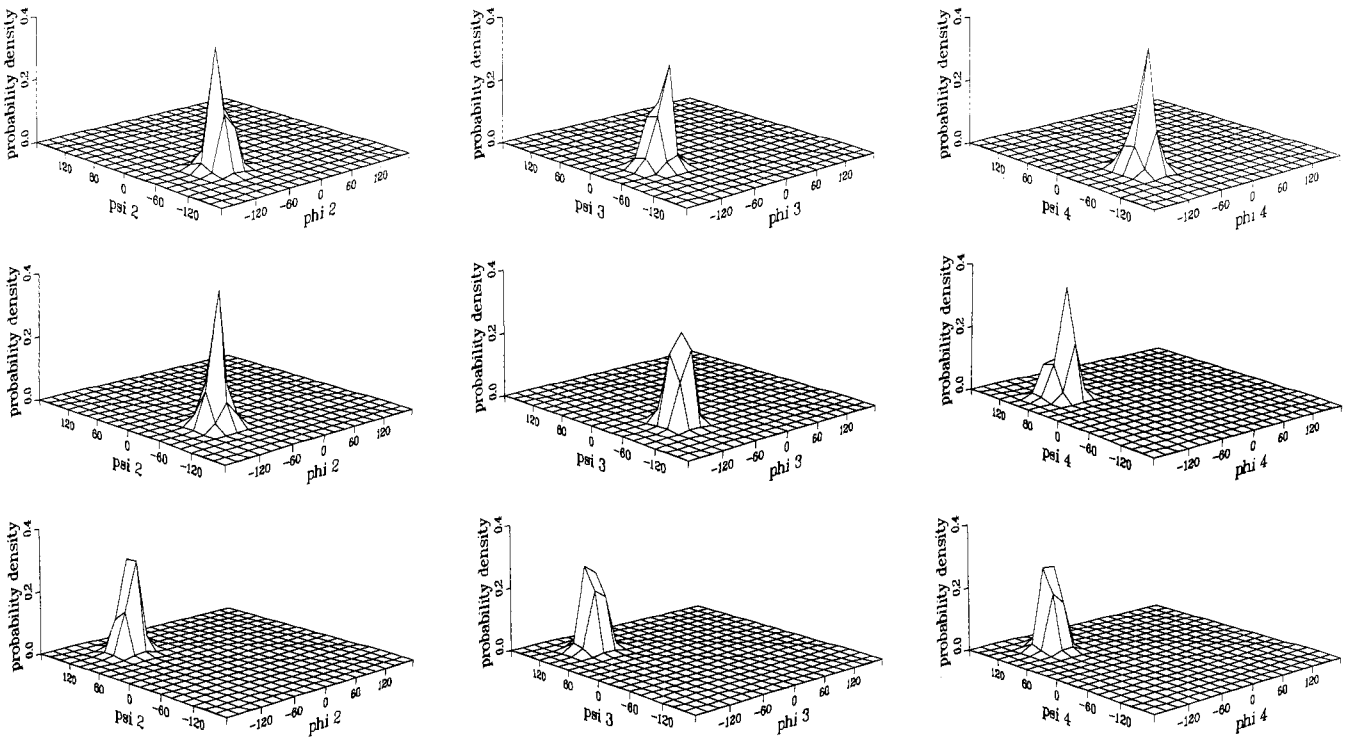

FIGURE 3: Normalized joint probability densities of the dihedral angle pairs (ϕ_2,ψ_2), (ϕ_3,ψ_3), and (ϕ_4,ψ_4) for Ac-(Val)$_3$-NHMe. The top set of distributions is from the r_0 = 2.2 Å simulation, the middle from the r_0 = 4.0 Å simulation, and the bottom from the r_0 = 9.2 Å simulation.

the hydrogen bonding in the turns, we looked at probability distributions (not shown) for the O_1–N_4 and O_2–N_5 distances. The distributions showed that the Ala peptide had 1–4 and 2–5 backbone hydrogen bonds, each for roughly 30% of the time, while the Val peptide was never hydrogen bonded. The biased probability distributions indicated $r(O_1$–$H_5)$ was in the range 3.8–4.5 Å for the Ala peptide and 4–5.5 Å for the Val peptide. Thus, those regions of the reaction coordinate correspond to two distinct ensembles of turn structures in Ac-(Ala)$_3$-NHMe and a single ensemble of turn structures in Ac-(Val)$_3$-NHMe during the r_0 = 4.0 Å simulations. When we carried out a similar analysis of the simulations with larger r_0, we found that turn structures also existed in both peptides for $r(O_1$–$H_5)$ = 5–6 Å. The three pairs of dihedral angles (distributions not shown) were in the α, α, and β regions, respectively, for both peptides, and the structures displayed chain reversals involving the first four residues (Figure 4D). However, these turns were more "open" than the smaller r-(O_1–H_5) turns, with their amide groups generally more exposed to the solvent (Figure 4D).

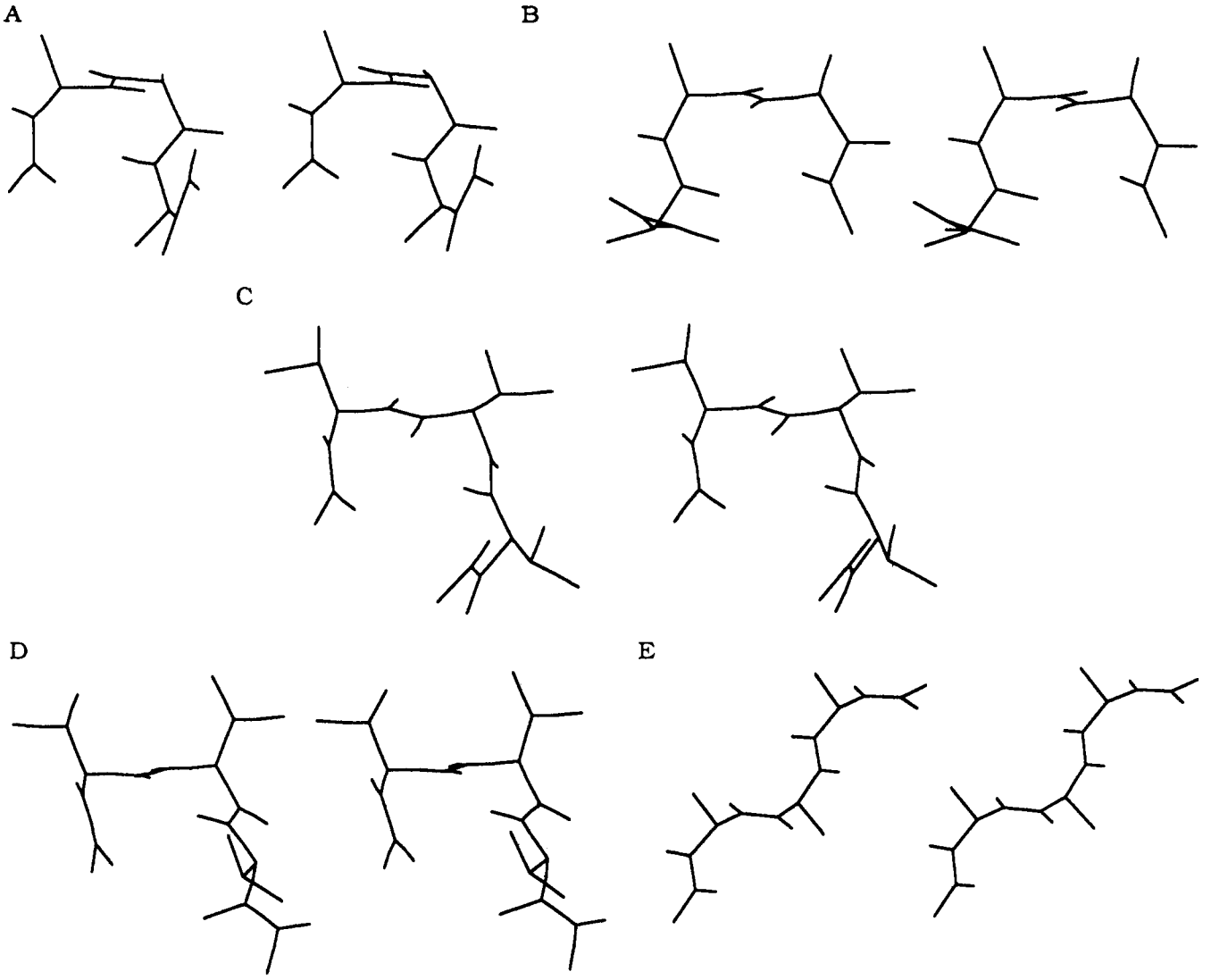

FIGURE 4: Stereoviews of representative structures along the helix unfolding reaction coordinate. (A) Reverse turn involving residues 1–4 from the r_0 = 4.0 Å simulation of Ac-$(Ala)_3$-NHMe. (B) Reverse turn involving residues 2–5 from the r_0 = 4.0 Å simulation of Ac-$(Ala)_3$-NHMe. (C) Reverse turn involving residues 1–4 from the r_0 = 4.0 Å simulation of Ac-$(Val)_3$-NHMe. (D) "Open" turn involving residues 1–4 from the r_0 = 6.0 Å simulation of Ac-$(Val)_3$-NHMe. (E) Extended structure from the r_0 = 10.2 Å simulation of Ac-$(Ala)_3$-NHMe. The molecular structures were drawn by the program MOLX (Sneddon, 1990).

Figures 2 and 3 show that the three pairs of dihedral angles remained in the β region during the r_0 = 10.2 Å simulation of Ac-$(Ala)_3$-NHMe and the r_0 = 9.2 Å simulation of Ac-$(Val)_3$-NHMe. Thus, the conformations were extended, like sections of β strand, with successive C–O bond vectors alternating in direction along the chain (Figure 4E). Molecular graphics analysis of the dynamics trajectories from these two simulations, and several other simulations with large r_0 values, showed that similar extended structures were generated throughout the range $r(O_1–H_5)$ = 9.5–11.5 Å for the Ala peptide and 8.5–10.5 Å for the Val peptide. In summary, our analysis of the peptide conformations along the reaction coordinate revealed that the region $r(O_1–H_5) \approx 2$ Å corresponds to helical conformations, ≈4–6 Å to reverse turns and ≈9–11 Å to extended structures.

In Figure 5 we show the free energy surfaces as functions of the reaction coordinate, $r(O_1–H_5)$, for Ac-$(Ala)_3$-NHMe and Ac-$(Val)_3$-NHMe. We joined the $W_i(r)$ from neighboring windows at the $r(O_1–H_5)$ values where the biased probability distributions intersected. Because the intersection between neighboring windows was quite large, most of the data used to compute the free energies came from the peaks of the distributions, and the statistical errors were therefore quite small. We obtained the statistical uncertainties as error propagated standard deviations in the free energies computed from blocks of 100 configurations. The uncertainties ranged from 0.2 to 0.3 kcal/mol for most of the $r(O_1–H_5)$ values to 0.5 kcal/mol near the end points. While the absolute vertical placement of the curves is arbitrary, we set them both to zero at $r(O_1–H_5)$ = 2.0 Å.

The pmfs in Figure 5 have several features in common. First of all, there is a narrow well centered at $r(O_1–H_5) \approx 2$ Å in each pmf. We showed above that when $r(O_1–H_5) \approx 2$ Å the peptides were in α helical conformations. Thus, these wells correspond to locally stable α helices in both peptides. Each pmf rises sharply for $r(O_1–H_5) < 2$ Å because of the van der Waals repulsion between the O_1 and H_5 atoms. As $r(O_1–H_5)$ is increased from 2 Å, there is a barrier in each pmf, followed by another well with a minimum at $r(O_1–H_5)$ = 4.2 Å for Ac-$(Ala)_3$HNHMe and 4.4 Å for Ac-$(Val)_3$-NHMe. We showed above that in the regions of these minima the peptides are in reverse-turn conformations. As $r(O_1–H_5)$ is increased from the reverse-turn minimum on each pmf, a second barrier is encountered at $r(O_1–H_5) \approx 6$ or 7 Å, followed by a broad deep well, corresponding to a manifold of stable extended conformations. The greater volumes of the turn and extended

Table I: Relative Thermodynamics of Helix, Turn, and Extended Conformations[a]

peptide	conformational change	ΔA	ΔE_{uu}	ΔE_{uv}	$-T\Delta S_{c,uv}$
Ac-$(Ala)_3$-NHMe	helix → turn A	1.6 ± 0.4	0.8 ± 6.4	6.5 ± 13.7	-5.8 ± 15.1
	helix → turn B	2.0 ± 0.3	6.8 ± 6.6	-4.3 ± 12.7	-0.5 ± 14.3
	helix → extended	-0.2 ± 0.3	-7.6 ± 5.8	10.9 ± 11.5	-3.5 ± 12.9
Ac-$(Val)_3$-NHMe	helix → turn A	-3.4 ± 0.3	3.2 ± 6.6	-0.2 ± 12.2	-6.4 ± 13.9
	helix → turn B	-3.2 ± 0.4	5.6 ± 7.9	-10.5 ± 13.0	1.7 ± 15.2
	helix → extended	-4.3 ± 0.3	-14.4 ± 6.6	27.2 ± 10.2	-17.1 ± 12.2

[a] Free energy contributions are in kcal/mol. The particular $r(O_1-H_5)$ values used for the helix, turn A, turn B, and extended conformations of Ac-$(Ala)_3$-NHMe were 2.0, 4.2, 5.6, and 10.2 Å, respectively, and those of Ac-$(Val)_3$-NHMe were 2.1, 4.4, 5.8, and 9.2 Å, respectively. The uncertainties were determined by error propagation from the standard deviations of averages over blocks of 100 configurations.

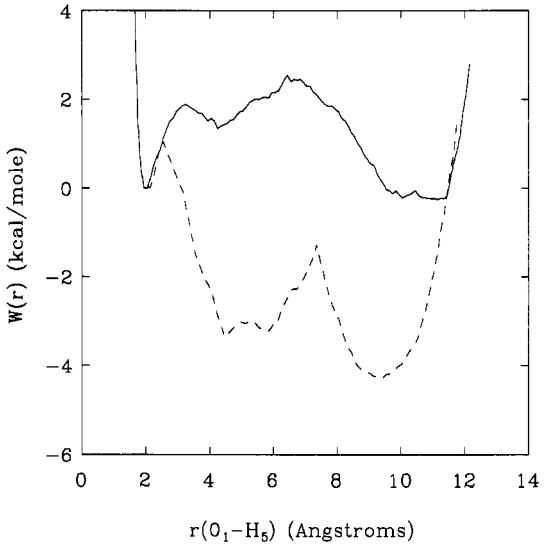

FIGURE 5: Free energy surfaces (potentials of mean force) as functions of the reaction coordinate $r(O_1-H_5)$. The solid curve is for Ac-$(Ala)_3$-NHMe, and the broken curve is for Ac-$(Val)_3$-NHMe. Both curves were arbitrarily set to zero at $r(O_1-H_5)$ = 2.0 Å.

wells compared to the helix wells shows that there are more stable turns and extended structures than helices, and hence the configurational entropies of the turn and extended states are greater. Finally, the steep walls at the large $r(O_1-H_5)$ sides of the extended state wells arise from bond-angle distortions produced by the constraint potential, and they represent the end of reasonable extended conformations on the reaction coordinate.

The pmfs suggest that the two peptides have vastly different helix–turn equilibria. The free energy barrier to the helix-to-turn transition in the Val peptide, which is at $r(O_1-H_5) \approx$ 2.6 Å and is about 1.1 kcal/mol high, is lower and sharper than that of the Ala peptide, which is at 3.2 Å and is 1.9 kcal/mol (Table II). The most striking difference between the two pmfs is in the character of the reverse-turn wells. The turn well for the Ala peptide is relatively shallow and is 1.4 kcal/mol higher in free energy than the Ala helix well, compared to the turn well for the Val peptide, which is broad and deep and is 3.3 kcal/mol lower than the Val helix well. Thus, helices are slightly more stable than reverse turns in Ac-$(Ala)_3$-NHMe, but they are much less stable than turns in Ac-$(Val)_3$-NHMe.

In contrast, the pmfs show that the equilibria between reverse turns and extended structures are much more similar in the two peptides. The free energy barrier for the turn-to-extended transition in the Ala peptide is about 1.2 kcal/mol and occurs at $r(O_1-H_5)$ = 6.4 Å (Table II). The barrier for the Val peptide, which is 2.1 kcal/mol at $r(O_1-H_5)$ = 7.2 Å, is slightly higher and sharper and occurs at a larger $r(O_1-H_5)$ distance. The lowest points in the turn wells for both peptides are located at $r(O_1-H_5) \approx$ 4.3 Å, but the center of the extended

Table II: Barrier Heights and Rate Constants for Conformational Transitions in Ac-$(Ala)_3$-NHMe and Ac-$(Val)_3$-NHMe

peptide	conformational change	$W^{\ddagger}$ [a]	k [b]
Ac-$(Ala)_3$-NHMe	helix → turn	1.9	0.042
	turn → helix	0.60	0.37
	turn → extended	1.2	0.14
	extended → turn	2.7	0.011
Ac-$(Val)_3$-NHMe	helix → turn	1.1	0.16
	turn → helix	4.4	0.00065
	turn → extended	2.1	0.030
	extended → turn	3.0	0.0067

[a] Free energy barrier heights in kcal/mol. [b] Transition-state theory rate constants in ps^{-1} at 300 K; $k = c \exp(-\beta W^{\ddagger})$, with c = 1 ps^{-1} (see Discussion).

well for the Val peptide occurs at about a 1 Å smaller O_1-H_5 separation than that of the Ala peptide. The free energy difference between the lowest points in the extended and turn wells is −1.3 kcal/mol for Ac-$(Ala)_3$-NHMe and −0.9 kcal/mol for Ac-$(Val)_3$-NHMe. The extended well for the Ala peptide has a greater volume and hence greater configurational entropy than the turn well, while for the Val peptide the volumes of the two wells are very similar. The greater configurational entropy of the extended state in the Ala peptide lowers its free energy slightly relative to the turn state. Overall, the pmfs predict that the ensemble of extended conformations is slightly more stable (by about 1 kcal/mol) than the ensemble of reverse turns in each peptide.

To determine quantitatively the relative stabilities of ensembles of helix, reverse turn, and extended conformations, we computed equilibrium constants using eq 2. We used the positions of the tops of the barriers (see Table II) separating the wells on the pmfs to define the limits of integration. For Ac-$(Ala)_3$-NHMe, we used the ranges $r(O_1-H_5) < 3.3$ Å for the helices, 3.3 Å $< r(O_1-H_5) <$ 6.4 Å for the turns, and $r(O_1-H_5) > 8.0$ Å for the extended conformations. This choice gave K_{eq} = 0.35 and ΔA = 0.6 kcal/mol for the helix-to-turn transition and K_{eq} = 4.3 and ΔA = −0.9 kcal/mol for the helix-to-extended transition. For Ac-$(Val)_3$-NHMe, we used the ranges $r(O_1-H_5) < 2.6$ Å for the helices, 2.6 Å $< r(O_1-H_5) <$ 7.2 Å for the turns, and $r(O_1-H_5) > 7.3$ Å for the extended conformations. This gave K_{eq} = 922 and ΔA = −4.1 kcal/mol for the helix-to-turn transition and K_{eq} = 4530 and ΔA = −5.0 kcal/mol for the helix-to-extended transition. These free energy differences computed from the equilibrium constants are similar to the values we obtain by simply taking differences between particular points in the wells on the pmfs (Table I). Thus, our results show qualitatively that the shapes of the wells on the pmfs (e.g., the configurational entropy contributions) have only a small influence on the relative stabilities of the stable conformations along the $r(O_1-H_5)$ coordinate. Therefore, the free energies differences given in Table I adequately reflect the "true" relative stabilities, as determined from the equilibrium constants.

To gain further insight into the microscopic interactions determining the relative stability of various structures along

the folding/unfolding coordinate [defined by *particular* values of $r(O_1-H_5)$], we have carried out thermodynamic decompositions of selected free energy differences according to eq 4 (Table I). We tabulated two turn–helix decompositions for each peptide in Table I because the decompositions were qualitatively different for turns with small and large values of $r(O_1-H_5)$. We refer to the smaller $r(O_1-H_5)$ turns as type A (see Figure 4A–C) and the more open, larger $r(O_1-H_5)$ turns as type B (see Figure 4D). We only tabulated one extended-helix decomposition for each peptide because the decompositions did not vary much throughout the extended state wells.

The decomposition of the extended-helix free energy difference is qualitatively similar for both peptides. Although the magnitude of each contribution is about twice as large for the Val peptide, the extended conformation of each peptide is strongly favored by the peptide–peptide energy and the peptide–water entropy and strongly opposed by the peptide–water energy. The net result is that the extended conformations are stabilized, by 0.2 kcal/mol for Ac-$(Ala)_3$-NHMe and 3.4 kcal/mol for Ac-$(Val)_3$-NHMe, relative to the helices.

The decompositions of the extended-helix energy differences are qualitatively similar to the decomposition of the free energy difference between extended conformations and hydrogen-bonded type I reverse turns in Ac-$(Ala)_2$-NHMe (Tobias et al., 1991a). The simple interpretation given previously by Tobias et al. (1991a) appears to work here as well. The line of reasoning goes as follows. The change in conformation from the compact, hydrogen-bonded structures (helices or type I turns) to extended structures is accompanied by a large negative change in peptide–peptide energy and a large positive change in peptide–solvent energy. These energy changes are dominated by their electrostatic contributions. In the compact conformations, the peptide dipoles are, for the most part, aligned in the same direction, while in the extended conformations they alternate in direction along the backbone. Thus, the peptide–peptide electrostatic interactions are more favorable in the extended conformations where the adjacent peptide dipoles cancel one another, and the peptide–solvent electrostatic interactions are more favorable in the compact conformations where the dipole moment of the whole molecule is greater. Moreover, the large positive changes in the peptide–water entropy, which amount to large negative entropic contributions to the free energy differences, arise because fewer water molecules are "bound" to the less polar extended conformations.

For the Ala peptide, the two types of turns are 1.6–2.0 kcal/mol less stable than the helix. The type A turn is very slightly destabilized relative to the helix by peptide–peptide interactions, strongly destabilized by the peptide–water energy, and strongly stabilized by the peptide–water entropic contribution. On the other hand, the type B turn is strongly destabilized by peptide–peptide interactions, strongly stabilized by the peptide–water energy, and only slighly stabilized by the peptide–water entropy. For the Val peptide, the two turns are 3.2–3.4 kcal/mol more stable than the helix. Both types of turns are substantially destabilized relative to the helix, type B more so than type A, by peptide–peptide interactions. The peptide–water energy is very slightly stabilizing and the entropy is strongly stabilizing for the type A turn, while the peptide–water energy is strongly stabilizing and the entropy is somewhat destabilizing for the type B turn.

The most obvious difference between Ac-$(Ala)_3$-NHMe and Ac-$(Val)_3$-NHMe evident from the pmfs is the helix-to-turn equilibrium. In principle, our thermodynamic decompositions allow us to identify the microscopic origins of this striking difference. Unfortunately, the energetic contributions to the turn–helix free energy changes are not all dominated by a single term (e.g., electrostatic), so the interpretation of the decompositions is not as simple as it was for the extended-helix changes. The main difference between the two peptides in the decomposition of the relative free energies of turn A and helix structures is in the peptide–water energetic contribution: the average peptide–water interaction energy difference is 6.5 kcal/mol for Ac-$(Ala)_3$-NHMe, compared to −0.2 kcal/mol for Ac-$(Val)_3$-NHMe. We looked at the contributions to these differences on an atom-by-atom basis and found that the electrostatic contribution from hydrogen-bonding groups (NH and CO) was 7.8 kcal/mol for Ac-$(Ala)_3$-NHMe and 3.9 kcal/mol for Ac-$(Val)_3$-NHMe. Using molecular graphics analysis, we found that these differences appeared to arise primarily from differences in peptide–water hydrogen bonding in the helix and turn states. These observations and the observation that the entropic contributions to the free energy differences are negative (e.g., the entropy difference is positive), imply that both peptides lose favorable hydrogen-bonding interactions with water when they undergo helix-to-turn A conformational changes. For the Ala peptide, the large positive electrostatic contribution dominates the turn–helix peptide–water interaction energy difference. For the Val peptide, the positive electrostatic contribution is offset by a van der Waals contribution of −4.1 kcal/mol, half of which is due to favorable van der Waals interactions of the side-chain C^γ methyl groups with water molecules. Thus, the main reason for the difference between the two peptides in the helix-to-turn A equilibria can be stated as follows: the loss of favorable hydrogen-bonding interactions in the turn A structures of the Val peptide is compensated by a net gain in favorable peptide–water packing interactions, mostly involving the Val side-chain methyl groups (we cannot tell from our data whether this net gain arises because unfavorable van der Waals interactions are lost or favorable interactions are gained in the turn A conformations of the Val peptide). Moreover, the Ala peptide suffers a net loss of favorable peptide–water electrostatic interactions, which is not compensated by a net gain of favorable peptide–water van der Waals interactions, upon a helix-to-turn A conformational change.

Although the structural differences between the type A and type B turns appear to be small [e.g., compared to the differences between either turn type and helices or extended structures (see Figure 4)], the decompositions of the turn–helix free energy differences for the type A turns are qualitatively different from those of the type B turns. However, once again, the largest difference between the two peptides is in the average peptide–water energetic contribution, which is −4.3 kcal/mol for Ac-$(Ala)_3$-NHMe and −10.5 kcal/mol for Ac-$(Val)_3$-NHMe. The electrostatic contributions from hydrogen-bonding groups is −0.3 kcal/mol for the Ala peptide and −4.5 kcal/mol for the Val peptide. This implies that the type B turn structure has, on the average, roughly the same number of hydrogen bonds to water as the helix in Ac-$(Ala)_3$-NHMe, but it has more than the helix in Ac-$(Val)_3$-NHMe. Our molecular graphics analysis supported this supposition. In addition, a net gain of favorable van der Waals interactions of the C^γ methyl groups with the water contributes −2.9 kcal/mol to the average peptide–water interaction energy difference between the turn B and helix structures in Ac-$(Val)_3$-NHMe. Thus, the main reason for the difference between the two peptides in the helix–turn B equilibria is that the turns in the Val peptide have effectively more hydrogen

bonds and favorable side-chain packing interactions with the solvent than the helix, leading to a large stabilization of the turn relative to the helix. In contrast, the stabilization of the turns due to peptide–water interactions is relatively small in the Ala peptide.

Discussion

Our pmfs predict that there are three major free energy minima, corresponding to stable ensembles of α helical, reverse turn, and extended structures, along a so-called helix folding/unfolding coordinate, $r(O_1–H_5)$, for both Ac-$(Ala)_3$-NHMe and Ac-$(Val)_3$-NHMe in water. The relative free energies, determined from the equilibrium populations of the stable structures, show that the extended states are the most stable for both peptides. Thus, strictly speaking, the helices and turns are actually "metastable" since, while they do have minima on the pmfs, they are not the most stable structures. This is in marked contrast to the situation observed previously in Ac-$(Ala)_2$-NHMe, where turn conformations similar to those observed in the present study not only are much higher (several kcal/mol) in free energy than extended conformations but also do not even have stable minima on the pmf along a similar folding/unfolding reaction coordinate (Tobias et al., 1991a). In Ac-$(Ala)_3$-NHMe, the helical state is slightly less stable (<1 kcal/mol) than the extended state, and the turn state is slightly less stable than the helical state, whereas in Ac-$(Val)_3$-NHMe the turn state is a little less stable ($\sim$1 kcal/mol) than the extended state, and the helical state is much less stable (several kcal/mol) than the turn state.

Our results may be used to predict a mechanism for helix initiation, and the reverse process, the conversion of one turn of an α helix to an extended "coil" state, in Ala and Val peptides along the particular pathway sampled by our constrained simulations. As the folding/unfolding coordinate, $r(O_1–H_5)$, is decreased from large values, the helix folding takes place in both peptides by successive $\beta \rightarrow \alpha$ transitions of the three pairs of backbone dihedral angles, in the order (ϕ_2,ψ_2), (ϕ_3,ψ_3), (ϕ_4,ψ_4). For each pair, the $\beta \rightarrow \alpha$ transition occurs almost exclusively by a change in ψ. In a sense, this is a "path of least conformational change" since substantial changes in the ϕ_i are not necessary to take a peptide from extended (all β) to helical (all α) conformations. The $\beta \rightarrow \alpha$ transitions in (ϕ_2,ψ_2) and (ϕ_3,ψ_3) occur in the region of the barrier separating the reverse-turn and extended structures on the pmfs for both peptides. The second transition involving (ϕ_3,ψ_3) results in stable reverse-turn structures for both peptides, and the final transition involving (ϕ_4,ψ_4) results in helices. The reverse turns are stable intermediates in the folding of the extended structures into one-turn α helices. If we assume that the unfolding mechanism is simply the reverse of this folding mechanism (which is justified if our simulations were carried out at equilibrium), then reverse turns are also important intermediates in the unfolding of one-turn helices. The structural transitions that occur along our folding/unfolding coordinate are similar to those observed along a minimum energy path (determined in a vacuum by using a distance-dependent dielectric constant to implicity represent the electrostatic screening due to water) connecting α helical and extended structures of isobutyryl-$(Ala)_3$-NHMe (Czerminski & Elber, 1989). We find it interesting that the reverse turns that result from the first (ϕ,ψ) transition from α to β correspond to a stable minimum along this minimum energy path.

Clearly, there are many other possible helix folding/unfolding pathways besides the one generated by our constrained simulations. Given the large number of important conformational degrees of freedom, it is impossible, in practice, to determine whether or not the particular pathway we studied is the "best" or "true" folding/unfolding pathway. Nonetheless, we do believe that our pathway is reasonable because our pmfs lead us to predictions that are consistent with the observations of other researchers. The mechanism we observed, which includes reverse turns as important intermediates along the helix folding/unfolding pathway, is consistent with the mechanism proposed by Sundaralingam and Sekharudu (1989), on the basis of their analysis of hydrated helices in protein crystal structures, and the mechanism observed by Tirado-Rives and Jorgensen (1990) in their simulations of helix unfolding in an S-peptide analogue. Some of the water-inserted helical turns observed in the former study and the 3_{10} helical intermediates observed during the formation and breakup of α helical hydrogen bonds in the latter study are similar to the reverse-turn intermediates observed in the present study. Finally, our pmfs predict that the helical content in the Val peptide is much lower than in the Ala peptide, in agreement with the results of the study by Padmanabhan et al. (1990) of the effects of nonpolar side-chain substitutions on the helix-forming tendencies of alanine-based peptides.

Regarding the role of solvation in the helix-to-turn equilibrium, the mechanism we observe differs from that proposed by Sundaralingam and Sekharudu (1989) and observed in the simulations of DiCapua et al. (1990). According to the predictions of Sundaralingam and Sekharudu, an α helical hydrogen bond is broken as follows: initially, a water molecule is externally bound to the CO group of the first residue in a turn of a helix; the water molecule then forms a three-centered hydrogen bond with the $C_i–O_i$ and $N_{i+4}–H_{i+4}$ groups; and finally, the water molecule disrupts the helical hydrogen bond by inserting between the $C_i–O_i$ and $N_{i+4}–H_{i+4}$ groups, and an $i,i+3$ hydrogen bond is formed, resulting in a reverse turn intermediate. This water insertion process was responsible for the disruption of a helical hydrogen bond in the middle of a deca-alanine helix during the simulation of DiCapua et al. (1990). Molecular graphics analysis of our simulation results showed that there is a water molecule externally bound to the CO group of the first residue in both peptides. However, as the $N_5–H_5$ group swings out (as the ψ_4 dihedral angle increases) during the helix-to-turn transition, the water molecule remains externally bound to the $C_1–O_1$ group rather than inserting between the $C_1–O_1$ and $N_5–H_5$ groups, and a different water molecule from the opposite side of the helix axis externally binds to the $N_5–H_5$ group. Thus, in our simulations, the NH and CO groups are solvated by different water molecules as the helix is disrupted. The differences in the solvation mechanisms observed by us and DiCapua et al. (1990) may be due to differences in the way the simulations were carried out: in our simulations the helices were unfolded by using constraints, whereas in the simulations of DiCapua et al. the helix disruption took place naturally. Alternatively, the differences may arise because we studied unfolding in a one-turn helix, whereas DiCapua et al. studied disruption at the middle of a 10-residue helix. The distribution of water molecules near the helical hydrogen bond in a one-turn helix, where there are several exposed NH and CO groups nearby, is certainly different than the distribution near a helical hydrogen bond in the middle of a helix. The differences in solvent distributions around the helical hydrogen bond could easily account for the differences in the solvation mechanisms.

Using our pmfs and transition-state theory (TST), we can make crude estimates of the time scales for helix folding/unfolding in Ac-$(Ala)_3$-NHMe and Ac-$(Val)_3$-NHMe in water. According to TST (Glasstone et al., 1941), the rate

constant is given by $k = c \exp(-\beta W^{\ddagger})$, where $W^{\ddagger}$ is the height of the free energy barrier to the process and c is the equilibrium average barrier crossing velocity. The TST rate is an upper bound to the "true" rate (or a lower bound to the time scale) because no corrections for multiple barrier crossings are included in the theory (Chandler, 1978). For lack of a better measure, we use $c \approx 10^{12}$ s^{-1}, which is the approximate value for side-chain rotation in a small protein (Northrup et al., 1982). For Ac-$(Ala)_3$-NHMe, we find that $k \approx 0.042$ ps^{-1} for the helix-to-turn transition and $k \approx 0.14$ ps^{-1} for the turn-to-extended transition at 300 K (Table II). For Ac-$(Val)_3$-NHMe, the corresponding values are $k \approx 0.16$ and 0.030 ps^{-1}, respectively. These values imply that the helix-to-turn and turn-to-extended transitions, and hence the unfolding one turn of a helix, occur roughly on a time scale of tens of picoseconds for both peptides. Our estimates are smaller than the time scales observed for the helix-to-turn transition at 278 K (~100 ps) and are similar to the time scale for the complete breakup of helical hydrogen bonds at 358 K (< 100 ps) in the simulations of Tirado-Rives and Jorgensen (1990). For the Ala peptide, we find $k \approx 0.011$ ps^{-1} for the extended-to-turn transition and $k \approx 0.37$ ps^{-1} for the turn-to-helix transition. For the Val peptide, the values are 0.0067 and 0.00065 ps^{-1}, respectively. These values imply that the extended-to-turn transition takes place in about 100 ps for both peptides and that the turn-to-helix transition occurs in a few picoseconds for the Ala peptide and about 1.5 ns for the Val peptide. Thus, we predict that helix initiation occurs on the time scale of 100 ps for Ac-$(Ala)_3$-NHMe and nanoseconds for Ac-$(Val)_3$-NHMe. These estimates are smaller than time scale for helix formation (10 ns–10 μs) estimated by Schwarz (1965) using a theoretical analysis of experimental helix–coil transition data but are similar to the time scale for reverse-turn formation in simulations of a pentapeptide in water (Tobias et al., 1991b).

Our results suggest that helix initiation in Ala and Val peptides is much easier than is predicted by the Zimm–Bragg theory with host–guest parameters. According to the theory (Zimm & Bragg, 1959), the equilibrium constant for the formation of one turn of a helix from a coil state is $K \approx \sigma s$, where σ is a "nucleation factor" and s is the equilibrium constant for adding a hydrogen bond to the helix. Using the host–guest parameters at 293 K (Wojcik et al. 1990), $K = 8.6 \times 10^{-4}$ for a one-turn helix in Ac-$(Ala)_3$-NHMe and $K = 9.5 \times 10^{-4}$ for a one-turn helix in Ac-$(Val)_3$-NHMe. With a two-state model [$K = f/(1-f)$, where f is the fraction of helix], these K values correspond to 0.086% helix for an Ala peptide and 0.0095% for a Val peptide. If we consider the coil state to be made up of only extended conformations [$r(O_1$–$H_5) > 6.4$ Å for Ac-$(Ala)_3$-NHMe and $r(O_1$–$H_5) > 7.6$ Å for Ac-$(Val)_3$-NHMe], then we get $K = 0.21$ for Ac-$(Ala)_3$-NHMe and $K = 2.4 \times 10^{-4}$ for Ac-$(Val)_3$-NHMe from our pmfs. Alternatively, if we consider the coil state to be composed of all conformations that are not α helical [$r(O_1$–$H_5) > 3.2$ Å for Ac-$(Ala)_3$-NHMe and $r(O_1$–$H_5) > 2.6$ Å for Ac-$(Val)_3$-NHMe], then we get $K = 0.23$ for Ac-$(Ala)_3$-NHMe and $K = 1.8 \times 10^{-4}$ for Ac-$(Val)_3$-NHMe. Thus, our K values are not very sensitive to the definition of the coil state. Using either set of K values and a two-state model, we predict ~20% helix in the Ala peptide and ~0.02% in the Val peptide. Our results predict that both peptides (but especially the Ala peptide) have a much larger K for helix initiation than is predicted by using the helix–coil transition theory with the host–guest parameters. Moreover, we predict a much greater difference in the K values between the two peptides than the theory predicts. We therefore conclude, as others have previously (Bierzynski et al., 1982; Marqusee & Baldwin, 1987; Marqusee et al., 1989, Padmanabhan et al., 1990), that the helix–coil theory with the host–guest parameters cannot generally be used to make reliable predictions of the stability of isolated short helices in solution.

If we consider the equilibrium constant for the coil-to-helix transition to be a measure of intrinsic helical propensity, then our results suggest that Ala has a 1000-fold greater helix initiation propensity (e.g., K for initiation) than Val. This agrees qualitatively with the results of Padmanabhan et al. (1990) in the sense that we predict that the helical content in a peptide with a high proportion of Val residues (in our case, all-Val) is much lower than in the all-Ala reference peptide. Furthermore, our prediction that the free energy of forming an Ala helix is less than that for a Val helix is consistent with the experimental work of O'Neil and DeGrado (1990) and Lyu et al. (1990) and the simulation study of Yun and Hermans (1990). A quantitative comparison is not possible, since our results are for helix initiation whereas the experimental results are most likely for helix propagation (Lyu et al., 1990).

It has been proposed that one reason why peptides with β branched side chains are less stable than their all-Ala counterparts has to do with the restriction of the branched side-chain rotamer conformations (Padmanabhan et al., 1990). The idea is that the conformations of β branched (and aromatic) side chains are restricted in a helix, and hence a helix with these side chains has less configurational entropy than an all-Ala helix. Since the configurational entropy of the helix is lower, the free energy is higher, and the helix with the branched side chains is destabilized relative to an all-Ala helix. In our simulations of the Ac-$(Val)_3$-NHMe helix, the conformations of the Val side chains were indeed restricted: the distributions of the χ_1 dihedral angle (defined by the N, C^{α}, C^{β}, and $C^{\gamma 1}$ atoms) were unimodal, narrow, and centered about 180° (e.g., with the γ methyl groups directly above the NH and CO groups) for residues 2 and 4, and –60° (e.g., staggered methyl groups) for residue 3. However, the χ_1 distributions were also unimodal and very narrow but centered about 180° for all three Val residues in our simulations of the extended Val peptide. Thus, the Val side-chain configurational entropy was similar in the helix and extended conformations. We therefore conclude, on the basis of our observations, that the restriction of the conformations of β branched side chains has little effect on the stability of the helices. Of course, it is conceivable that alternate important conformations of the Val side chains were not sampled during our simulations. Yun et al. (1990) have carried out a detailed simulation study employing special sampling of all the possible side-chain conformations in an alanine helix with a single Val residue. They found that the destabilization of the helix relative to an all-Ala helix due to side-chain conformational restriction is small (~0.5 kcal/mol).

It has also been proposed that β branched side chains can destabilize the unfolded state through entropic effects (Nemethy et al., 1966; Dao-Pin et al., 1990). Evidently, a branched side chain such as Val restricts the backbone conformations more than a small side chain such as Ala. Therefore, the unfolded state of a peptide with a Val residue has less configurational entropy, and hence is destabilized (leading to a net stabilization of the helix), compared to its all-Ala counterpart. If this effect is appreciable, it should show up in our pmfs: the free energy minimum of the extended state of Ac-$(Val)_3$-NHMe should be noticeably narrower than that of Ac-$(Ala)_3$-NHMe, reflecting the reduced flexibility of the

unfolded state in the Val peptide. Indeed, the extended state well of the Val peptide is slightly narrower than that of the Ala peptide (Figure 5). However, we estimate that the net stabilization of the Val helix relative to the Ala helix due to this entropic effect is very small (< 0.5 kcal/mol). Nemethy et al. (1966) estimated that this entropic effect would destabilize the unfolded state by ~0.7 kcal/mol when Val is substituted for Ala.

Previous work has also suggested that another reason why β branched side chains have a relatively low frequency in helices in proteins (e.g., compared to Ala), and hence are helix destabilizing, is because of unfavorable steric interactions of the γ methyl groups with the backbone in a helix (O'Neil & DeGrado, 1990). We investigated the possible role of these interactions in our simulations of Ac-$(Val)_3$-NHMe. None of the average peptide–peptide interaction energy differences between the helices and either of the turns or the extended structures had a component that indicated a loss of unfavorable van der Waals interactions or relief of bond or angle strain (created by unfavorable steric interactions), upon undergoing a helix-to-turn or extended conformational transition. Thus, the Val side-chain methyl groups did not appear to significantly destabilize helical conformations during our simulations of Ac-$(Val)_3$-NHMe. Yun et al. (1990) estimated that the destabilization due to steric interactions when an Ala residue is replaced by Val in an all-Ala helix is quite small (~0.5 kcal/mol).

Unfortunately, insofar as helix initiation is concerned, our results suggest that the large difference between the helical propensities of Ala andVal cannot be explained by simple concepts such as side-chain rotamer restriction or unfavorable steric interactions. Rather, the origin of the difference appears to be quite complicated because it involves subtle differences in the solvation of the two peptides. The two peptides have similar turn–extended equilibria but very different helix–turn equilibria, and the difference in helical propensities reflects the fact that the helix–turn equilibrium strongly favors the turns in Ac-$(Val)_3$-NHMe, while it favors the helices in Ac-$(Ala)_3$-NHMe. Our thermodynamic decompositions revealed that the helix–turn equilibria are vastly different primarily because the changes in peptide–water interactions that accompany helix-to-turn conformational changes are qualitatively different for the two peptides. Undoubtedly, the subtle differences in the solvation of particular residues in various conformations are strongly sequence dependent, and this may partially explain the apparent sequence dependence of helical propensities noted by Padmanabhan et al. (1990).

In this paper, we have concentrated on the initiation stage of α helix formation. However, to develop a more complete microscopic picture of helix formation, we must also examine the propagation stage. It has been known for a long time that the helix–coil transition is highly cooperative (Doty et al., 1954). This cooperativity implies that it is much easier to form a helical hydrogen bond once an adjacent one has been formed and, therefore, that propagation is easier than initiation (Zimm & Bragg, 1959). To quantitatively assess the differences between the initiation and propagation stages of helix formation, we are currently using simulations to study the thermodynamics of the formation of one hydrogen bond in water at both the N- and C-termini of α helices with two hydrogen bonds.

ACKNOWLEDGMENTS

We are grateful to the Pittsburgh Supercomputing Center for a generous grant of computer time allocated by the N.S.F. We are very grateful to Scott Sneddon for many interesting and helpful discussions regarding this work.

REFERENCES

Allen, M. P., & Tildesley, D. J. (1989) *Computer Simulation of Liquids*, p 24, Oxford University Press, Oxford.
Barlow, D. J., & Thornton, J. M. (1988) *J. Mol. Biol. 201*, 601.
Bierzynski, A., Kim, P. S., & Baldwin, R. L. (1982) *Proc. Natl. Acad. Sci. U.S.A. 79*, 2470.
Blagdon, D. E., & Goodman, M. (1975) *Biopolymers 14*, 241.
Bradley, E. K., Thomason, J. F., Cohen, F. E., Kosen, P. A., & Kuntz, I. D. (1990) *J. Mol. Biol. 215*, 607.
Brooks, B. R., Bruccoleri, R. E., Olafson, B. D., States, D. J., Swaminathan, S., & Karplus, M. (1983) *J. Comput. Chem. 4*, 187.
Chandler, D. (1978) *J. Chem. Phys. 68*, 2959.
Chou, P. Y., & Fasman, G. D. (1977) *J. Mol. Biol. 115*, 135.
Czerminski, R., & Elber, R. (1989) *Proc. Natl. Acad. Sci. U.S.A. 86*, 6963.
Dao-Pin, S., Baase, W. A., & Matthews, B. W. (1990) *Proteins 7*, 198.
DiCapua, F. M., Swaminathan, S., & Beveridge, D. L. (1990) *J. Am. Chem. Soc. 112*, 6768.
Doty, P., Holtzer, A. M., Bradbury, J. H., & Blout, E. R. (1954) *J. Am. Chem. Soc. 76*, 4493.
Dyson, H. J., Rance, M., Houghten, R. A., Wright, P. E., & Lerner, R. A. (1988) *J. Mol. Biol. 201*, 201.
Fairman, R., Shoemaker, K. R., York, E. J., Stewart, J. M., & Baldwin, R. L. (1989) *Proteins 5*, 1.
Glasstone, S., Laider, K. J., & Eyring, H. (1941) *The Theory of Rate Processes*, McGraw-Hill, New York.
Goodman, E. M., & Kim, P. S. (1989) *Biochemistry 28*, 4343.
Jorgensen, W. L., Chandrasekhar, J., Madura, J., Impey, R. W., & Klein, M. L. (1983) *J. Chem. Phys. 79*, 926.
Kabsch, W., & Sander, C. (1983) *Biopolymers 22*, 2577.
Karplus, M., Ichiye, T., & Pettitt, B. M. (1987) *Biophys. J. 52*, 1083.
Kim, P. S., & Baldwin, R. L. (1982) *Annu. Rev. Biochem. 51*, 459.
Kim, P. S., Bierzynski, A., & Baldwin, R. L. (1982) *J. Mol. Biol. 162*, 187.
Lyu, P. C., Liff, M. I., Marky, L. A., & Kallenbach, N. R. (1990) *Science 250*, 669.
Marqusee, S., & Baldwin, R. L. (1987) *Proc. Natl. Acad. Sci. U.S.A. 84*, 8898.
Marqusee, S., Robbins, V. H., & Baldwin, R. L. (1989) *Proc. Natl. Acad. Sci. U.S.A. 86*, 5286.
Nemethy, G., Leach, S. J., & Scheraga, H. A. (1966) *J. Phys. Chem. 70*, 998.
Northrup, S. H., Pear, M. R., Lee, C.-Y., McCammon, J. A., & Karplus, M. (1982) *Proc. Nat. Acad. Sci., U.S.A. 79*, 4035.
O'Neil, K. T., & DeGrado, W. F. (1990) *Science 250*, 646.
Osterhout, J. J., Jr., Baldwin, R. L., York, E. J., Stewart, J. M., Dyson, H. J., & Wright, P. E. (1989) *Biochemistry 28*, 7059.
Padmanabhan, S., Marqusee, S., Ridgeway, T., Laue, T. M., & Baldwin, R. L. (1990) *Nature 334*, 268.
Ptitsyn, O. B., & Rashin, A. A. (1975) *Biophys. Chem. 3*, 1.
Richardson, J. S. (1981) *Adv. Protein Chem. 34*, 167.
Richmond, T. J., & Richards, F. M. (1978) *J. Mol. Biol. 119*, 537.
Roder, H., Elove, G. A., & Englander, S. W. (1988) *Nature 335*, 700.
Ryckaert, J.-P., Ciccotti, G., & Berendsen, H. J. C. (1977) *J. Comput. Phys. 23*, 327.

Schiffer, M., & Edmundson, A. B. (1967) *Biophys. J. 7*, 121.
Schwarz, G. (1965) *J. Mol. Biol. 11*, 64.
Shoemaker, K. R., Kim, P. S., Brems, D. N., Marqusee, S., York, E. J., Chaiken, I. M., Stewart, J. M., & Baldwin, R. L. (1985) *Proc. Natl. Acad. Sci. U.S.A. 82*, 2349.
Shoemaker, K. R., Kim, P. S., York, E. J., Stewart, J. M., & Baldwin, R. L. (1987) *Nature 326*, 563.
Sneddon, S. F. (1990) MOLX Series of Molecular Graphics Programs, Department of Chemistry, Carnegie Mellon University.
Sundaralingam, M., & Sekharudu, Y. C. (1989) *Science 244*, 1333.
Tirado-Rives, J., & Jorgensen, W. L. (1991) *Biochemistry 30*, 3864.
Tobias, D. J., Sneddon, S. F., & Brooks, C. L., III (1991a) *J. Mol. Biol. 216*, 783.
Tobias, D. J., Mertz, J. E., & Brooks, C. L., III (1991b) *Biochemistry 30*, 6054–6058.
Udgaonkar, J. B., & Baldwin, R. L. (1988) *Nature 335*, 694.
Valleau, J. P., & Torrie, G. M. (1977) in *Statistical Mechanics, Part A* (Berne, B. J., Ed.) p 169, Plenum, New York.
Verlet, L. (1967) *Phys. Rev. 159*, 98.
Wojcik, J. Altmann, K.-H., & Scheraga, H. A. (1990) *Biopolymers 30*, 121.
Yun, R. H., & Hermans, J. (1990) *Proteins* (submitted).
Zichi, D. A., & Rossky, P. J. (1986) *J. Chem. Phys. 84*, 1712.
Zimm, B. H., & Bragg, J. K. (1959) *J. Chem. Phys. 31*, 526.

Action of a Microbial Lipase/Acyltransferase on Phospholipid Monolayers†

Suzanne Hilton and J. Thomas Buckley*
Department of Biochemistry and Microbiology, University of Victoria, Box 1700, Victoria, British Columbia V8W 2Y2, Canada
Received January 4, 1991; Revised Manuscript Received April 4, 1991

ABSTRACT: *Vibrio* species release a lipase which shares many properties with mammalian lecithin–cholesterol acyltransferase. We have studied the action of the enzyme on phospholipid monolayers. At similar surface pressures, reaction velocities were higher with monolayers of dilauroylphosphatidylcholine than with the corresponding phosphatidylglycerol or phosphatidylethanolamine. The dependence of reaction velocity on molecular density was very similar for phosphatidylcholine and phosphatidylethanolamine monolayers. Lag times were shortest with phosphatidylglycerol at low molecular densities, but maximum velocity was reached at considerably lower densities than with the other two lipids. We have found [Hilton, S., McCubbin, N. D., Kay, C., & Buckley, J. T. (1990) *Biochemistry 29*, 9072–9078] that nicking of the enzyme with trypsin or other proteases results in an increase in its activity against lipids in membranes. Here we show that trypsin treatment results in a large change in the surface activity of the lipase, allowing it to penetrate monolayers at pressures higher than 40 $mN \cdot m^{-1}$.

All of the lipases characterized so far appear to be members of a superfamily of esterases which are capable of catalysis at lipid–water interfaces (Kirchgessner et al., 1987, 1989; Komaromy & Schotz, 1987; Wion et al., 1987; Persson et al., 1989). Under the right conditions, lipases will hydrolyze virtually any ester bond, in contrast to the phospholipases, which are often highly specific for the polar head groups of their substrates. In addition, many lipases are active in nonaqueous systems where they may also catalyze stereospecific ester formation (Harwood, 1989). These attributes have generated considerable recent interest as well as proposals for a variety of biotechnological applications. In spite of this, the reaction mechanisms of these enzymes are not well understood. On the basis of active-site sequence homology with the serine proteases (Maraganore & Heinrikson, 1986), the structures of two lipases determined by X-ray crystallography (Winkler et al., 1990; Brady et al., 1990), and some circumstantial evidence obtained by chemical modification (Burstein et al., 1974; Jauhiainen & Dolphin, 1986; De Caro et al., 1989), it is generally assumed that the lipases all have a Ser-His-Asp amino acid triad at the active site. However, there is little direct evidence to support this assumption and no explanation for the differences in specificities and reaction rates which are observed among these enzymes.

The microbial glycerophospholipid–cholesterol acyltransferase (GCAT) and mammalian lecithin–cholesterol acyltransferase (LCAT) both contain short amino acid sequences homologous to the consensus sequence of the lipase superfamily (Maraganore & Heinrikson, 1986; Komaromy & Schotz, 1987; Persson et al., 1989). Like the other lipases, they will hydrolyze ester linkages at lipid–water interfaces, but they are distinguished by their ability to carry out acyl transfer from phospholipids to cholesterol in lipoproteins, bilayers, and inverted micelles (Buckley et al., 1982, 1984; Buckley, 1982, 1983). In addition, there is some evidence that their reaction mechanisms may differ from those of the other lipases. Thus, it has been suggested that at least one cysteine plays a role in LCAT-catalyzed acyl transfer (Jauhiainen & Dolphin 1986; Jauhiainen et al., 1988), and we have shown recently by site-directed mutagenesis that although the serine in the lipase consensus sequence of GCAT is absolutely required for activity, none of the histidines in the enzyme participate in hydrolysis or acyl transfer (Hilton & Buckley, 1990).

We have also shown that, under certain assay conditions, proteolytic nicking results in a profound increase in the activity of GCAT (Hilton et al., 1990). The bacterium releases the

† Supported by grants from the British Columbia Heart Foundation and the National Science and Engineering Research Council.

0006-2960/91/0430-6070$02.50/0